A Sliding Mode Virtual Sensor for Wheel Forces Estimation with Accuracy Enhancement via EKF

E. Regolin, A. Alatorre, M. Zambelli, A. Victorino, A. Charara, A. Ferrara, *Senior Member, IEEE*

***Abstract*—An algorithm for the estimation of the longitudinal and lateral forces exerted at wheel level between tires and ground is presented. Starting from a modified version of the single track vehicle model, which also includes the steady-state effect of pitch and roll on the planar movement of the vehicle, the structure is designed as a cascade of two Sub-Optimal Second Order Sliding Mode (S-SOSM) observers, featuring an adaptive feedback which helps improving the accuracy of the estimation of the longitudinal forces. The presented approach is purposely designed so that only standard sensors, which are usually available in commercial vehicles, are exploited. In order to alleviate the high frequency vibrations introduced by the Sliding Mode technique, an EKF is added as a second step, which considers the output of the S-SOSM observer as a noisy measurement, hence the virtual sensor nomenclature. The method is evaluated on experimental data, displaying good performance both in terms of accuracy and chattering alleviation.**

***Index Terms*—Vehicle dynamics, Sliding mode control, Forces estimation, Extended Kalman Filter**

I. Introduction

The automotive industry has made significant improvements in last decades addressing passenger safety, driving quality and energetic efficiency. Recently, with the introduction of on-board automatic control systems, this trend has increased its momentum exponentially. One example of this trend is the amount of first-event rollovers for single-vehicle crashes, which has decreased considerably. For instance, as reported in [1], in the USA it went from 4.29% in 2004 to 2.61% in 2010. In this example, the improvement can be ascribed to the introduction of the Electronic Stability Control (ESC) system. Another meaningful case is that of vehicles equipped with Anti-lock Braking System and ESC, which run off the road almost 50% less than vehicles without this equipment, see [2].

Within the scope of active safety control systems and energy efficiency topics, the estimation of tire-ground contact forces has become an important subject of investigation. In fact, the knowledge of the forces exerted can help to prevent over-steering or under-steering phenomena, which often generate accidents. This can be caused by a tire undergoing excessive slip/skid, so that the driver does not reach the intended trajectory. Currently, sensors exist able to measure tire-ground forces. Nevertheless, their cost amounts to several tens thousand euros per piece, which makes them incompatible with commercial automobiles mass production. The introduction of observers to estimate these forces is an effective solution for this problem. However, to provide estimates of the forces with sufficient accuracy is still considered an arduous task, since the variation of vehicle mass, Center of Gravity (COG) position, road slope or bank angle, along with road irregularities and load transfer effects increase the problem complexity considerably.

Accurate knowledge of vehicle dynamics is therefore essential to accomplish the task of determining the wheel forces with suitable accuracy to be used in Advanced Driver Assistance System (ADAS) and ESC systems. Motivated by this necessity, numerous research works have been published concerning the estimation of vehicle parameters and forces [3]–[6]. Conversely, on the side of energetic efficiency, recent vehicle controllers developed for fuel consumption reduction require an accurate estimation of the vehicle traction force [7]–[10].

A. Related Work

In general, the computation or estimation of the tire-ground forces can follow two main approaches, both having their own advantages. The first one requires the development of a tire model, while the second one uses the vehicle dynamic model to reconstruct the tire forces. The tire model approach [11], [12] is useful during the tire design, while its application within an embedded system is in general problematic.

For this reason, several authors developed the idea of computing the tire-ground forces using a tireless model approach, which only considers the vehicle dynamics. One of the first examples can be found in [13], where a nonlinear state and tire-ground force observer is developed, and applied to a braking control system. In that paper, the tire-ground forces are computed relying on a single-track model (bicycle model) of the car [14]. The use of an Extended Kalman Filter (EKF), is widely popular in this field of application. An example can be found in [15], where an EKF is used to calculate the tire-ground forces for the wheels of the bicycle model. Sliding Mode (SM) based observers have been also employed. In [16], for instance, the estimation process is subdivided into two steps. As a first step, a SM observer is applied to a bicycle model while, as a second step, the response is refined with an EKF. Yet, as for the aforementioned approaches, the computation of the forces is done for the virtual tires of the bicycle model, not for the real tires of the vehicle. In [17], a Kalman filter is used to estimate the forces at each wheel, under the hypothesis of equal distribution for forces on the same axle. In [18] a similar approach is presented in which, in order to avoid such assumption, the motor torque and

E. Regolin, M. Zambelli and A. Ferrara are with the Dipartimento di Ingegneria Industriale e dell'Informazione, University of Pavia, via Ferrata 5, 27100 Pavia, Italy (e-mail: [enrico.regolin - massimo.zambelli - a.ferrara]@unipv.it)

A. Alatorre, A. Victorino and A. Charara are with Université de Technologie de Compiègne, France (e-mail: [angalato - alessandro.victorino - ali.charara]@hds.utc.fr)

the braking torque are considered as known input variables. In [19], the longitudinal and lateral force transfer concept is introduced. This term improves the accuracy of the force decoupling step. In [20], the longitudinal tire-ground forces are computed and the longitudinal force transfer is redefined giving the estimator robustness against changes in tire-ground friction. More recently, in [21], an individual tire force estimation algorithm designed for all wheel drive vehicles was proposed. Using the interacting multiple model (IMM) filter method, the suggested algorithm helps avoiding the chattering response caused by immediately switching between different vehicle dynamic models.

SM concept based solutions to the problem of tire-ground forces estimation have well documented advantages, in terms of fast response and stability, and drawbacks, such as the so-called chattering effect and the strong dependance on model accuracy, when implemented in observers [22]. In particular, when a First Order Sliding Mode (FOSM) is used, from a theoretical point of view the observer output corresponds to the desired estimation only in the so called "Filippov's sense" [23], as will be described in Section III.

From the above mentioned works, it emerges that approaches which rely on a single-track vehicle dynamic model and exploit a SM based observation law are typically affected by a number of problems, which to this day still represent a research topic in the field of wheel forces estimation. These issues, which we propose to address in this work, include:

- allocation of the wheel forces relative to the same axle;
- calibration of the SM gains for chattering minimization;
- unreliability of the wheel torque information;
- precise estimation of the longitudinal forces for the non-driving wheels.

B. Contribution and Outline

In this paper we present a novel observers based scheme for wheel forces estimation which, analogously to some of the previously mentioned works, exploits the sinergy of SM observers and the EKF. The presented proposal differs from the previous ones for several reasons.

- It relies on the concept of Second Order Sliding Mode (SOSM) to design the observers. In particular, the proposed observers provide estimates which are determined via a Sub-Optimal SOSM (S-SOSM) [24] observer law. By choosing it over a classical FOSM law, one theoretically should not need to filter the observer input signal in order to obtain the estimated values while in sliding, since this signal is by construction continuous. In practice, this implies a considerable attenuation in the chattering level. The S-SOSM algorithm adopted in this paper also presents other interesting features, both in terms of robustness and convergence time, which enable to achieve superior performance compared to the SM concepts.
- In this work we use an enhanced single-track vehicle model, also including the yaw moment due to the vehicle load transfer, which makes the estimation design more complex, but enables to obtain results more consistent with real world signals evolution.
- The use of the EKF is done in a different perspective in the proposed scheme with respect to the work mentioned before. In the previously mentioned work [16] a 2 layers observer is developed, so that the first SM observer produces estimates for the tire-ground forces, which are then fed to the second EKF layer, which is in charge of estimating related variables, such as side-slip angles and stiffness coefficients. As a result, no smoothing of the vibrations in the estimated forces is actually performed. In this work, instead, the EKF is coupled with the S-SOSM observers in order to further reduce the possible residual chattering affecting the estimations.
- With the proposed scheme, an adaptive mechanism based on the estimation of the losses due to aerodynamic drag and friction is introduced in order to obtain a further improvement in terms of accuracy.

To the best of our knowledge, the proposed approach is original and has not been applied yet to solve the automotive estimation problem in question. In view of its significant accuracy and robustness, it also seems suitable for practical realization of a virtual sensor which can complement the physical sensors of an automated 4-wheeled vehicle.

This article is structured as follows. Section II describes the vehicle model used for the development of the observer, while in III some theoretical background on the used S-SOSM algorithm is introduced. An overview of the presented scheme is given in Section IV, before analyzing in depth the S-SOSM implementation and its stability properties (Section V). The implementation of the EKF and the method employed for the inclusion of nonlinear phenomena affecting non driving wheels are illustrated in Section VI. Finally, the performance of the observers, evaluated on experimental data, is presented in Section VII, before the conclusions are drawn in VIII.

II. Vehicle Model

The goal of the proposed observer is to estimate longitudinal and lateral forces exerted on each wheel, based on available information, such as measurements obtained from sensors and known vehicle parameters. A key part of this procedure is the adoption of a valid vehicle model, which should take into account the main dynamic effects concurring to the generation of such forces. At the same time it is necessary that the model complexity remains reasonable, in order to guarantee that all the considered states are sufficiently excited during the estimation, and all parameters utilized in the model are reliable, thus ensuring an appropriate level of robustness. For this reason, some phenomena, such as tire relaxation, need to be neglected.

Based on the aforementioned considerations, the main aspects considered in the adopted vehicle model are the following:

- wheel rotational dynamics, described by the "single corner model";
- vehicle dynamics, described by an enhanced version of the "single track model";
- longitudinal and lateral load transfer.

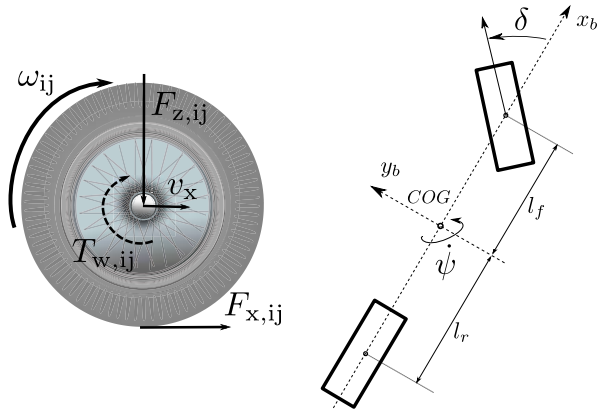

(a) Single Corner Model (b) Single Track Vehicle Model

Figure 1. Graphical representation of the quantities involved in the adopted models.

In the next few subsections the mentioned models are presented. Note that, in order to help the reader, the following notation will be used throughout the article:

$$F_{\nu\eta,ij}, \quad \nu \in \{x,y\}; \quad \eta \in \{w,b\}; \quad i \in \{f,r\}; \quad j \in \{l,r\} \tag{1}$$

where x, y indicate longitudinal and lateral quantities, respectively, and w, b indicate the wheel or vehicle body reference frames. The subscripts ij specify the wheel indexing (forward/rear, left/right). In case of the lateral forces only, with the notation $F_{by,f}$ and $F_{by,r}$ we refer to the lateral forces applied to the front and rear axles, respectively.

A. Single Corner Model

The longitudinal forces $F_{\mathrm{xw,ij}}$ exerted on the ij-th wheel are modelled after the first equation of the so-called single-corner model (see Fig. 1(a), and [25]), which considers the dynamics of a single wheel with respect to its own reference frame

$$J_{\mathrm{w}}\dot{\omega}_{\mathrm{ij}} = (T_{\mathrm{w,ij}} + \Delta T_{\mathrm{w,ij}}) - R_{\mathrm{e}}F_{\mathrm{xw,ij}}, \tag{2}$$

where J_{w}, ω_{ij}, R_{e} are the moment of inertia, the angular speed and the effective radius of the wheel, respectively, $T_{\mathrm{w,ij}}$ is the torque acting on the wheel, and $F_{\mathrm{xw,ij}}$ is the longitudinal force. Note that, for all i, j, equalities $R_{\mathrm{e,ij}} = R_{\mathrm{e}}$ and $J_{\mathrm{w,ij}} = J_{\mathrm{w}}$ are assumed throughout the paper. Nevertheless, the validity of the model is independent of the actual values of the effective radius and wheel moment of inertia, which are assumed available, so that this does not represent a limitation.

The additional term $\Delta T_{\mathrm{w,ij}}$, is introduced, in order to take into account the inaccuracies in the information concerning the actual torque applied to the wheel. For conventional vehicles in particular, and to a lesser extent for the increasingly popular electrical ones, the measurement/estimation of the actual torque applied to a specific wheel, both in the case of a power-on situation and during braking, is not a trivial task. In fact, the mechanical/hydraulic transfer of power to the wheels is affected by several external agents, such as temperature, aging, malfunctioning, etc. [26]. Note that, the form in which (2) is expressed is such that, if a device for the estimation of $\Delta T_{\mathrm{w,ij}}$ is introduced, in practice all matched uncertainties affecting the model will be compensated as if they were a unique uncertain term, including also parametric uncertainties.

B. Enhanced Single Track Model

The lateral forces are taken into account, referring to the vehicle reference frame, starting from the so-called single-track planar model (see Fig. 1(b), [14], [27] for reference). The single-track model is in general used to describe the planar motion of a vehicle, by considering the dynamic evolution of three variables representing its degrees of freedom. Typically the three variables used are longitudinal velocity v_{x}, lateral velocity v_{y} (alternatively absolute velocity and side-slip angle), and yaw rate $\dot{\psi}$.

The model is valid under the hypothesis that the forces applied are homogeneous along the axles, so that it can be assumed that all forces are exerted by a unique wheel, placed at the center of the axle itself. For this reason, the bicycle model is not particularly indicated to describe the vehicle dynamics occurring during sharp turns, when the vehicle load transfer is most felt. As a matter of fact, when a significant lateral load transfer occurs, it makes sense to consider the effect it has on the difference between longitudinal forces on the wheels of the same axle, which in turn contributes to the generation of the overall yaw moment. For this reason, in this paper a modified version of the single track model is considered, which takes into account the yaw moment induced by such force difference

$$\begin{cases} \dot{v}_{\mathrm{x}} = \frac{1}{m}\left[(\sum_{\mathrm{i,j}} F_{\mathrm{xb,ij}}) - F_{\mathrm{aer}} - F_{\mathrm{rr}} + g\sin(\theta)\right] \\ \dot{v}_{\mathrm{y}} = \frac{1}{m}(\sum_{\mathrm{i,j}} F_{\mathrm{yb,ij}}) (= a_{\mathrm{y}}) \\ \ddot{\psi} = \frac{1}{J_{\mathrm{z}}}(l_{\mathrm{f}}F_{\mathrm{yb,f}} - l_{\mathrm{r}}F_{\mathrm{yb,r}}) + \frac{1}{2J_{\mathrm{z}}}(b_{\mathrm{f}}\Delta F_{\mathrm{xb,f}} + b_{\mathrm{r}}\Delta F_{\mathrm{xb,r}}) \end{cases} \tag{3}$$

The first equation in (3) will be exploited in an adaptive loop, which is one of the peculiar aspects of our proposal, oriented to improve the quality of the forces estimation, and which requires an estimation of the main longitudinal losses due to aerodynamic drag and rolling resistance. For this purpose, with the wheels longitudinal forces referred to the vehicle body $F_{\mathrm{xb,ij}}$, the balance of forces concurring to the evolution of the vehicle velocity is considered, where the overall rolling resistance is defined as

$$F_{\mathrm{rr}} = C_{\mathrm{r}}mg \tag{4}$$

and the aerodynamic drag is

$$F_{\mathrm{aer}} = \frac{1}{2}\rho C_{\mathrm{x}}v_{\mathrm{x}}^2 \tag{5}$$

having introduced the rolling resistance coefficient C_{r} and the longitudinal drag coefficient C_{x}. Note that, while the rolling resistance is a phenomenon occurring at the level of the wheels, in this approach it is preferred to consider its effect on the vehicle dynamics.

In the second and third equations in (3) the following terms

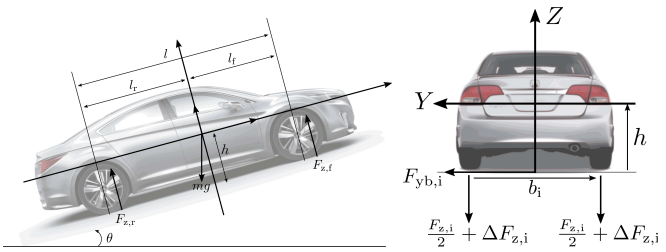

(a) (b)

Figure 2. (a) Front and rear axles load distribution (b) load shift of the i-th axle

are considered

$$\begin{cases} F_{\mathrm{yb,f}} = F_{\mathrm{yb,fl}} + F_{\mathrm{yb,fr}} \\ F_{\mathrm{yb,r}} = F_{\mathrm{yb,rl}} + F_{\mathrm{yb,rr}} \\ \Delta F_{\mathrm{xb,f}} = F_{\mathrm{xb,fr}} - F_{\mathrm{xb,fl}} \\ \Delta F_{\mathrm{xb,r}} = F_{\mathrm{xb,rr}} - F_{\mathrm{xb,rl}} \end{cases} \tag{6}$$

where J_z is the vehicle total moment of inertia, l_f, l_r are the distances of the front and rear axles from the center of gravity, and b_f, b_r are the distances between the two wheels of the same (front or rear) axle. The term $\frac{1}{2J_z}(b_\mathrm{f}\Delta F_{\mathrm{xb,f}} + b_\mathrm{r}\Delta F_{\mathrm{xb,r}})$ is considered in order to represent the effects of the longitudinal forces on the overall yaw moment generation, i.e. the moment generated by the differences in the longitudinal forces acting on the wheels of the same axle ($\Delta F_{\mathrm{xb,k}}$).

C. Load Transfer

If only the enhanced single track and single corner models were used, there would be no information on how the forces are allocated on the wheels of the same axle. As a matter of fact, the load transfer, which determines a varying distribution of the normal forces on the 4 wheels, is not included in the planar model (3). For this reason, an approach for the approximation of the effects of the load transfer, both longitudinal and lateral, based on the information provided by the accelerometers rather than on dynamic equations, is presented here.

The introduction of two equations relative to pitch and roll is needed in order to take into account the load transfer occurring during the maneuvers and due to the inclination of the road. For both pitch and roll phenomena, the steady state values are considered, i.e. the derivatives of the pitch and roll angles are assumed to be null.

Regarding the pitch, the vehicle must be considered as a 2-D object moving in the $X - Z$ plane, defined by the longitudinal and vertical axes (see Fig. 2(a)). Given the purpose of this paper, it is sufficient to only consider the components affecting more heavily the weight transfer. This means that several minor causes for longitudinal transfer are neglected, mainly:

- the displacement of the resulting normal forces from the center of contact of the tires (the ones responsible for the rise of the rolling resistance);
- the effect of the total aerodynamic moment about the Y axis;
- the effect of the aerodynamic drag on the longitudinal load transfer;

This leaves the following simplified calculation for the distribution of the normal forces on the axles $F_{\mathrm{z,i}}$

$$\begin{cases} F_{\mathrm{z,f}} = \frac{1}{l_\mathrm{f}+l_\mathrm{r}}\left(l_\mathrm{r} mg\cos(\theta) - mg\sin(\theta)h - a_\mathrm{x} mh\right) \\ F_{\mathrm{z,r}} = \frac{1}{l_\mathrm{f}+l_\mathrm{r}}\left(l_\mathrm{f} mg\cos(\theta) + mg\sin(\theta)h + a_\mathrm{x} mh\right) \end{cases} \tag{7}$$

where the longitudinal inclination angle θ of the road can be estimated based on vision sensors or inertial measurement units, so that the term $mg\sin(\theta)$ can always be computed.

Expression (7) only provides the total forces acting on each axle, whereas the final aim is to obtain the normal forces acting on each wheel. The steady state effects of vehicle roll are then considered, assuming for the sake of simplicity that the road presents no lateral slope. Since the assumption of rigid body does not allow to compute the load transfer acting on each axle, the compliance of the suspensions is introduced. The following conclusions are based on a detailed description of the vertical dynamics effect, which can be found in [14]. Having defined k_i as the stiffness of the suspensions of the i-th axle, one has the following expression for the lateral weight transfer:

$$\Delta F_{\mathrm{z,i}} = -\frac{k_\mathrm{i}}{b_\mathrm{i}} h \frac{\sum_\mathrm{i} F_{\mathrm{yb,i}}}{\sum_\mathrm{i} k_\mathrm{i}} \tag{8}$$

This leads to the final expression

$$\begin{cases} F_{\mathrm{z,il}} = \frac{F_{\mathrm{z,i}}}{2} - \frac{k_\mathrm{i}}{b_\mathrm{i}} h \frac{\sum_\mathrm{i} F_{\mathrm{yb,i}}}{\sum_\mathrm{i} k_\mathrm{i}} \\ F_{\mathrm{z,ir}} = \frac{F_{\mathrm{z,i}}}{2} + \frac{k_\mathrm{i}}{b_\mathrm{i}} h \frac{\sum_\mathrm{i} F_{\mathrm{yb,i}}}{\sum_\mathrm{i} k_\mathrm{i}} \end{cases} \tag{9}$$

in which the $F_{\mathrm{z,i}}$ terms are defined in (7).

III. S-SOSM for Control and Observation

Sliding Mode control (SM) [28] is a robust nonlinear control technique based on the idea of exploiting Variable Structure Systems (VSS) properties in order to constrain the system trajectory to a predefined subset of the state space. In this section, this technique is briefly outlined in order to clarify its role in our proposal. Note that, in the paper, the dependance of variables on time t is omitted, apart from non obvious cases.

A. Sub-Optimal Second Order Sliding Mode

Consider a system affine in the control

$$\dot{x} = f(x,t) + g(x,t)u \tag{10}$$

where $x \in \mathbb{R}^n$, $u \in \mathbb{R}$, and $f(x,t)$ and $g(x,t)$ are two uncertain bounded vector functions. A "sliding variable" $\sigma = \sigma(x,t)$ has to be designed as a function of states and possibly time. Although in principle it can assume any form, a common choice is the linear time-invariant one

$$\sigma(x) = Cx(t), \tag{11}$$

with $C \in \mathbb{R}^{1\times n}$ constant. Considering σ as a system output, the relative degree r of system (10)-(11) is defined as the order of the total time derivative of σ in which the control u appears explicitly for the first time [29]. For systems with $r = 1$ it is sufficient to rely on the application of First-Order Sliding Mode (FOSM) control laws such as, for instance,

$$u = -K\,\mathrm{sign}(\sigma). \tag{12}$$

For a proper choice of the gain K, in fact, discontinuous laws as (12) ensure that the trajectory of (10) reaches in finite time the sliding manifold

$$\sigma = 0 \quad \in \mathbb{R}^{(n-1)} \tag{13}$$

and remains confined on it $\forall t \geq t_r$, t_r being the reaching time.

For systems with relative degree two ($r = 2$), instead, at least a second order sliding modes must be enforced (i.e. the trajectory of system (10) is constrained in finite time on the sliding set $\{\sigma = 0,\ \dot{\sigma} = 0\}$). The dynamics of the sliding variable in such cases can be described by the following perturbed chain of integrators,

$$\begin{cases} \dot{\zeta}_1 = \zeta_2 \\ \dot{\zeta}_2 = \lambda(\zeta_1, \zeta_2) + D(\zeta_1, \zeta_2)v \end{cases} \tag{14}$$

where $\zeta_1 = \sigma$, $\zeta_2 = \dot{\sigma}$, v is the control, and λ and D are two continuous uncertain functions such that

$$\begin{cases} |\lambda(\zeta_1(t), \zeta_2(t))| < \Lambda \\ 0 < D_1 < D(\zeta_1(t), \zeta_2(t)) < D_2 \end{cases} \tag{15}$$

with Λ, D_1 and D_2 being known constants*. The second inequality in (15) can be substituted by $D_1 < D < D_2 < 0$ if the sign of the (16) is negative.

In this work the S-SOSM control algorithm [24] is considered. It aims at making σ and $\dot{\sigma}$ vanish in finite time by means of the control law

$$v = -\alpha K \operatorname{sign}\left(\sigma - \frac{\sigma_{\mathrm{MAX}}}{2}\right), \tag{16}$$

where α is a modulation parameter, K is the gain and $\sigma_{\mathrm{MAX}} = \sigma(t_{\mathrm{MAX}})$ with t_{MAX} the last time instant at which $\dot{\sigma} = 0$.

To implement an n-th order sliding mode control law, the knowledge of the first $n-1$ time derivatives of the sliding variable is usually mandatory. This increases the complexity of the resulting schemes, in which additional sensors or differentiators must be introduced. On the contrary, one of the peculiarities of S-SOSM is that no derivatives of σ are needed, as can be seen in (16). In fact, in real implementations, σ_{MAX} can be determined using commercial peak detectors or looking at successive measurements of σ. If the difference $\Delta\sigma_i = \sigma(t_i) - \sigma(t_{i-1})$ between the last two acquired values has opposite sign with respect to $\Delta\sigma_{i-1}$, it means that $\dot{\sigma} = 0$ happened. This is an approximation, which implies that some non-idealities are introduced in practice with respect to a perfect knowledge of $\dot{\sigma}$, but they are typically tolerable.

The selection of K and α must fulfill the following conditions

$$\alpha = \begin{cases} \alpha^* & \text{if } \left(\zeta_1 - \frac{1}{2}\zeta_{\mathrm{MAX}}\right)(\zeta_{\mathrm{MAX}} - \zeta_1) > 0 \\ 1 & \text{otherwise} \end{cases} \tag{17}$$

$$K > \max\left(\frac{\Lambda}{\alpha^* D_1}; \frac{4\Lambda}{3D_1 - \alpha^* D_2}\right) \tag{18}$$

with $\alpha^* \in (0, 1] \cap \left(0, \frac{3D_1}{D_2}\right)$ a parameter to be arbitrarily chosen and ζ_{MAX} obviously related to σ_{MAX} [24], in order to guarantee the finite-time convergence of σ and $\dot{\sigma}$ to zero. Note that, in this paper, it is assumed for simplicity that there is no uncertainty affecting the D term in (14), so that $D_1 = D_2 = D$ and $\alpha^* = 1$.

A feature of S-SOSM is that it can be exploited also to control systems of relative degree one, for chattering alleviation. In such cases, the control can be applied to an augmented system whose relative degree is artificially increased from $r = 1$ to $r = 2$ by means of the introduction of an integrator, so that the discontinuous control law v affects the actual control variable evolution as

$$\dot{u} = v. \tag{19}$$

Equation (19) guarantees that the real control signal u is continuous, so that chattering (i.e. the high frequency oscillations of σ due to the control discontinuity) is attenuated. From now on, in this work we will only consider the application of S-SOSM in its chattering alleviation form, on systems of relative degree $r = 1$.

The Sliding Mode approach can be easily applied to external disturbances observation tasks. Let us assume that the system dynamics are described by

$$\dot{x} = f_k(x, t) + f_u(x, t) \tag{20}$$

where $f_k(x, t)$ and $f_u(x, t)$ are, respectively, a known and unknown functions of state and time. The latter, in particular, can comprise unmodeled dynamics, exogenous disturbances and non-idealities of any kind. If the state vector x is available for measurement, the observer system

$$\dot{\hat{x}} = f_k(x, t) + \hat{u} \tag{21}$$

can be constructed, where $\hat{u}$ is the observer input. Then, the sliding variable can be chosen as

$$\sigma = x - \hat{x}. \tag{22}$$

During a second order sliding, the following equality holds

$$\sigma = \dot{\sigma} = \dot{x} - \dot{\hat{x}} = f_u(x, t) - \hat{u} = 0 \tag{23}$$

and, therefore, $\hat{u} = f_u(x, t)$. Note that this feature is a peculiar property of the S-SOSM approach. In case a First Order Sliding Mode approach were used to design $\hat{u}$, equality (23) would be true only in Filippov's sense [23] (i.e. $\hat{u}$ would be discontinuous, and only its "equivalent" counterpart would be equal to $f_u(x, t)$ [28]).

B. Convergence Time

The enforcement of a second-order sliding mode proves to be equivalent to the regulation of system (14). In [24] the proof that law (16) enforces a contractive behavior of the state of (14) towards the origin, under (17), (18), is provided. The contraction of the state (14) implies that the successive values of the peak σ_{MAX} respect

$$|\sigma_{\mathrm{MAX_{i+1}}}| < |\sigma_{\mathrm{MAX_i}}|, \quad i = 1, 2, \ldots \tag{24}$$

and finite time convergence follows. In particular, an upper bound for the reaching phase duration can be computed as

$$\bar{t}_r = \lim_{k \to \infty} t_{\mathrm{MAX_k}} < \frac{\beta'}{1 - \gamma} + t_{\mathrm{MAX_1}} \tag{25}$$

*Note that we implicitly assume to know the sign of D (say, positive) and that $D \neq 0$.

where $t_{\mathrm{MAX_k}}$ is the time instant at which the k-th peak detection occurs. Therefore, $t_{\mathrm{MAX_1}}$ is such that $\dot{\sigma} = 0$ for the first time. Relationship (25) is determined considering the following inequality (see [24] for more details):

$$\begin{aligned} t_{\mathrm{MAX_{k+1}}} &< \beta \sum_{\mathrm{i}=1}^{k} \sqrt{|\sigma_{\mathrm{MAX_i}}|} + t_{\mathrm{MAX_1}} \\ &= \beta \sum_{\mathrm{i}=1}^{k} \gamma^{i-1} \sqrt{|\sigma_{\mathrm{MAX_1}}|} + t_{\mathrm{MAX_1}} \end{aligned} \tag{26}$$

in which $0 < \gamma < 1$ is used as a coefficient in the geometric series originated by Inequality (24) and

$$\beta = \frac{(D_1 + \alpha^* D_2)K}{(D_1 K - \Lambda)\sqrt{\alpha^* D_2 K + \Lambda}} \tag{27}$$

In order to simplify (26), then, β' is defined as

$$\beta' = \beta \sqrt{|\sigma_{\mathrm{MAX_1}}|} \tag{28}$$

Notice that the parameter γ appearing in (25) depends on the magnitude of the disturbances. In particular, zero being its lower bound, an upper bound can be found considering that the following relationship holds between each peak and its preceding one (see [24])

$$|\sigma_{\mathrm{MAX_{i+1}}}| < \mu |\sigma_{\mathrm{MAX_i}}| \tag{29}$$

so that, eventually,

$$0 < \gamma < \sqrt{\mu} < 1 \tag{30}$$

IV. SM Virtual Sensor with Accuracy Enhancement

In [30] wheel forces are estimated by means of an observer, structured as the cascade of two S-SOSM observers for the longitudinal and lateral forces, with an adaptive feedback loop for the correction of the longitudinal forces estimation. While designs have already been proposed for wheel forces estimation, exploiting both first and second order sliding mode techniques (see e.g. [31], [32]), the motivation for the adoption of the S-SOSM in [30] is to alleviate the chattering produced. For this reason, also a switched/time-based algorithm (STBA) is adopted for the adaptation of the gain, based on the method proposed in [33].

The simulation results reported in [30] are satisfactory, yet the method requires a high computational burden for the off-line calibration of the STBA algorithm, which is based on the optimization of several parameters corresponding to different regions of the phase plane and to the associated gains. Moreover, by optimizing the calibration over an increasing number of scenarios, the chattering level corresponding to optimum increases. This aspect could be dealt with, by further increasing the number of regions in which the phase plane of the sliding variable is subdivided, although this would come at the cost of additional parameters, and thus with an exponentially increasing computational load for the calibration.

The approach which is presented in this article is substantially different: while the base S-SOSM observer is still employed, the task of chattering alleviation is assigned to an EKF, which, together with the sensor measurements, which are naturally noisy, acquires the estimations $\hat{F}_{xw,ij}$, $\hat{F}_{y,i}$, $i = f, r$, $j = l, r$, and considers them as if they were also obtained from noisy sensors. In the latter case, the noise is indeed represented by the chattering generated by the Sliding Mode approach.

The immediate consequence of such implementation is that there is a reduced benefit from a decrease in the S-SOSM gains. In turn, the calibration focus shifts towards a proper tuning of the observation covariance matrix R of the EKF. One key advantage of this evolution is the fixed number of calibration parameters. In fact, with the STBA method [34], there is no a-priori knowledge of the optimal number of regions in which the $(\sigma, \dot{\sigma})$ phase-plane should be divided to get an efficient chattering alleviation. Conversely, with the EKF, the number of parameters to be calibrated depends on the dimension of the observed state.

A second feature which was not originally present in [30] is the inclusion in the adopted model of the load transfer when performing the lateral forces allocation between wheels of the same axle. This solution allows, with limited computational effort, and without the need for a dynamic model for pitch and roll dynamics, to vastly improve the performance of the estimation, in conditions where the lateral dynamics are under intense excitation.

Finally, the EKF smoothing capability allows to feed the S-SOSM virtual sensor with unfiltered measurement signals, since the noise cancellation results in being performed at a second stage. In this way, the S-SOSM observers are not working with already delayed signals, which is a significant advantage for accuracy.

V. S-SOSM Based Virtual Sensor for Wheel Forces

A. S-SOSM Observer Structure

The vehicle models introduced in Section II are now exploited for the derivation of the forces observer. Moreover, in order to limit the excess of notation, it will be assumed that the road slope is negligible, so that the approximation $\theta \approx 0$ is valid.

The longitudinal forces $F_{\mathrm{xw,ij}}$ are estimated relying on the dynamic description of the rotation of each wheel, which is provided by model (2). Assuming that the nominal values of J_{w}, R_{e} are known, the measured wheel speed ω_{ij} and the requested wheel torque T_{ij} are suitably used to generate a S-SOSM which implies the vanishing of the error

$$\sigma_{\mathrm{x,ij}} = \omega_{\mathrm{ij}} - \hat{\omega}_{\mathrm{ij}} \tag{31}$$

This is done by controlling the estimation law

$$J_{\mathrm{w}} \dot{\hat{\omega}}_{ij} = T_{\mathrm{w,ij}} - \hat{\Delta T}_{\mathrm{ij}} - R_{\mathrm{e}} u_{\mathrm{x,ij}} \tag{32}$$

where u is the observer input law designed according to (16), (19). As a result, one has that the estimated force is $\hat{F}_{\mathrm{xw}} = u_{ij}$. Note that, the torque deviation $\hat{\Delta T}_{ij}$ is derived from the overall torque deviation term $\hat{\Delta T}$. Its distribution over the 4 wheels is calculated differently in accelerating and braking situations. The assumption which is made is that if no torque is applied to a specific wheel, the corresponding torque deviation is negligible. Consequently, since the usecase considered in the experimental

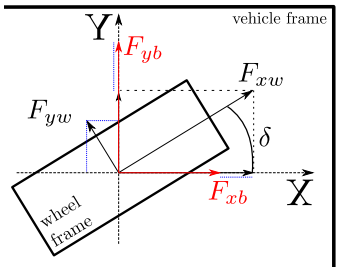

Figure 3. Front-left wheel forces representation

evaluation in Section VII is a conventional vehicle with front wheels traction, $\hat{\Delta T}$ is distributed as follows:

$$\hat{\Delta T}_{\mathrm{ij}} = \begin{cases} \hat{\Delta T}\frac{\hat{F}_{\mathrm{z,fj}}}{\hat{F}_{\mathrm{z,f}}} & \text{if } a_{\mathrm{x}} > a_{\mathrm{thd}} \quad \text{acceleration} \\ \hat{\Delta T}\frac{\hat{F}_{\mathrm{z,ij}}}{mg} & \text{if } |a_{\mathrm{x}}| < a_{\mathrm{thd}} \quad \text{coasting} \\ \hat{\Delta T}\frac{\hat{F}_{\mathrm{z,ij}}}{mg} c_{\mathrm{brk,ij}} & \text{if } a_{\mathrm{x}} < -a_{\mathrm{thd}} \quad \text{braking} \end{cases} \tag{33}$$

where the normal forces distribution is derived from (9), the coefficients $c_{\mathrm{brk,ij}}$ account for the brake torque split ratio, and the acceleration threshold a_{thd} is calibrated in order to minimize high frequency oscillations in the identification of the driving modes acceleration, coasting and braking.

We assume that $\hat{\Delta T}$ is provided by a PI adaptive law

$$\dot{\hat{\Delta T}} = K_P \dot{e}_{\mathrm{F_x}} + K_I e_{\mathrm{F_x}}, \tag{34}$$

with the input error $e_{\mathrm{F_x}}$ given by

$$e_{\mathrm{F_x}} = ma_{\mathrm{x}} - \left(\sum_{\mathrm{ij}} (\hat{F}_{\mathrm{xb,ij}}) - \hat{F}_{\mathrm{aer}} - \hat{F}_{\mathrm{rr}} \right) \tag{35}$$

where $\hat{F}_{\mathrm{aer}}$ and $\hat{F}_{\mathrm{rr}}$ are derived from the models (4) and (5), respectively. Since the vehicle velocity is required for the estimation of $\hat{F}_{\mathrm{aer}}$, a one dimensional Kalman Filter is used for its derivation, exploiting measured acceleration and wheel speeds as inputs and outputs, respectively.

One can notice how the estimation of the longitudinal wheel forces performed according to (31) and (32) is referred to the wheels reference frame: this means that in order to preserve validity when a non-null steering angle δ is applied to the front wheels (see Fig. 3), a linear transformation has to be performed to calculate the forces summation in (35). Typically, the steering angle δ has a limited range of admitted values, and therefore the following assumption can be considered valid

$$\cos(\delta) \gg 0 \tag{36}$$

Considering the front-left wheel, one has

$$\begin{cases} F_{\mathrm{xb,fl}} = cos(\delta) F_{\mathrm{xw,fl}} - sin(\delta) F_{\mathrm{yw,fl}} \\ F_{\mathrm{yb,fl}} = sin(\delta) F_{\mathrm{xw,fl}} + cos(\delta) F_{\mathrm{yw,fl}} \end{cases} \tag{37}$$

which can be expressed in matrix form as

$$\begin{bmatrix} F_{\mathrm{xb}} \\ F_{\mathrm{yb}} \end{bmatrix} = Q(\delta) \begin{bmatrix} F_{\mathrm{xw}} \\ F_{\mathrm{yw}} \end{bmatrix} \tag{38}$$

First and second equation in (37) can be combined by eliding $F_{\mathrm{yw,fl}}$, so that the following expression for $F_{\mathrm{xb,fl}}$ is obtained

$$\begin{aligned} F_{\mathrm{xb,fl}} &= \left(cos(\delta) + \frac{sin^2(\delta)}{cos(\delta)} \right) F_{\mathrm{xw,fl}} - \frac{sin(\delta)}{cos(\delta)} F_{\mathrm{yb,fl}} \\ &= \frac{1}{cos(\delta)} F_{\mathrm{xw,fl}} - tan(\delta) F_{\mathrm{yb,fl}} \end{aligned} \tag{39}$$

The transformation (38) is then modified into the form considered in the observation scheme in Fig. 4, i.e.

$$\begin{bmatrix} F_{\mathrm{xb}} \\ F_{\mathrm{yw}} \end{bmatrix} = \underline{Q}(\delta) \begin{bmatrix} F_{\mathrm{xw}} \\ F_{\mathrm{yb}} \end{bmatrix} \tag{40}$$

By extending the same approach to the front-right wheel all terms required for the summation in (35) are obtained.

The lateral forces are estimated based on the modified single track model (3) previously illustrated. Thanks to the fact that with such an approach the lateral forces on the same axle are considered homogeneous, the model dynamics are reduced to a single equation, so that a single S-SOSM observer can be used. The forces, referred to the body reference frame, concur to generate the lateral acceleration of the vehicle as follows

$$ma_{\mathrm{y}} = F_{\mathrm{yb,f}} + F_{\mathrm{yb,r}} \tag{41}$$

where it is assumed that a_{y} is available for measurement by means of an accelerometer. The S-SOSM observer is designed so that the following estimation error is steered to zero in finite time

$$\sigma_{\mathrm{y}} = \dot{\psi} - \dot{\hat{\psi}} \tag{42}$$

Note that, in (42), $\dot{\hat{\psi}}$ and $\hat{F}_{\mathrm{yb,f}}$ are defined as follows

$$\begin{cases} \ddot{\hat{\psi}} = \frac{1}{J_z}[l_{\mathrm{f}} ma_{\mathrm{y}} - (l_{\mathrm{f}} + l_{\mathrm{r}}) u_{\mathrm{y}} + \frac{1}{2} b_{\mathrm{f}} \Delta \hat{F}_{\mathrm{xb,f}} + \frac{1}{2} b_{\mathrm{r}} \Delta \hat{F}_{\mathrm{xb,r}}] \\ \hat{F}_{\mathrm{yb,f}} = ma_{\mathrm{y}} - u_{\mathrm{y}} \end{cases} \tag{43}$$

where $\Delta \hat{F}_{\mathrm{xb,f}}$, $\Delta \hat{F}_{\mathrm{xb,r}}$ are derived from (6). As a result, and in analogy with the longitudinal case, one has that the estimated force acting on the rear axle is $\hat{F}_{\mathrm{yb,r}} = u_{\mathrm{y}}$, with u_{y} also designed according to (16).

The estimation of the lateral forces on each quarter-car, differently from the implementation presented in [30], is not obtained by equally splitting the axle force $F_{\mathrm{yb,i}}$ on the two corresponding wheels. While the approximation of equal distribution is reasonable when the difference between the normal forces acting on the wheels of the same axle is small, for more aggressive turns, the performance of the observer drops dramatically. For this reason, similarly to the approach followed in [19], the lateral forces are assigned depending on the normal forces distribution

$$\hat{F}_{\mathrm{yb,ij}} = \hat{F}_{\mathrm{yb,i}} \frac{\hat{F}_{\mathrm{z,ij}}}{\hat{F}_{\mathrm{z,il}} + \hat{F}_{\mathrm{z,ir}}} \tag{44}$$

Note that, such solution is in analogy with the torque deviation $\hat{\Delta T}$ distribution in equation (33). The overall scheme which represents the observer is illustrated in Fig. 4, comprehensive of the three components which have been illustrated.

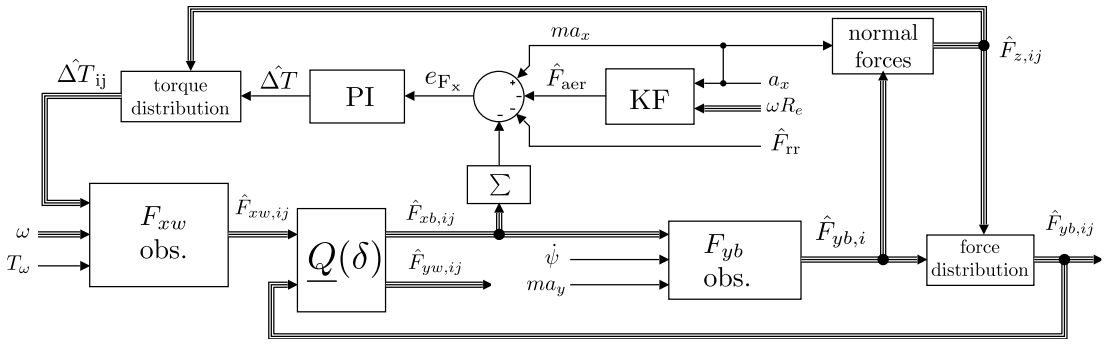

Figure 4. The complete observation scheme, where $\underline{Q}(\delta)$ is the matrix representing the linear transformation from (40)

B. Convergence Analysis

From a theoretical viewpoint, the observation errors of observer systems (32) and (43) can be proved to converge to zero as required, by exploiting the principle of "control hierarchy" illustrated by DeCarlo in [35]. Considering the cascade of longitudinal and lateral observers as a unique multi-input system, by following DeCarlo's approach, the overall finite time convergence is guaranteed by a suitable choice of the gains, as will be discussed in the following. First we need to discuss the effect of the feedback adaptive loop on the performance of the observer for the longitudinal forces.

In fact, the two observers represent the main element in the scheme in Fig. 4, where the PI logic is a practical device adopted in order to increase the accuracy of the estimation, by considering all the possible information available to the observer. In this case the PI component produces an adaptive estimation of the torque distortion term $\hat{\Delta T}$, which is introduced in order to take into account all uncertainties related to the vehicle longitudinal dynamics. Due to the nonlinearity of the system upon which the PI feedback law is applied, a proof of its convergence properties is not straightforward. Nevertheless, one can notice how the S-SOSM observers converge in finite time to an estimation, which, although bounded, is affected by possible distortions on the input signals. Since the terms $\Delta T_{\rm ij}$ are in practice a correction to the input torque value $T_{\rm w,ij}$, one can say that they do not affect the stability of the cascade, as long as the observer gain K_x is defined taking into account the maximum amplitude that their derivatives can assume.

By considering the derivative $\dot{\hat{\Delta T}}$ of the output of the PI controller, given by (34), one can see that its value is bounded, as long as the input error $e_{\rm F_x}$ is bounded and has bounded derivative. This can be proved straightforward, considering that the rate of change of the estimated forces is indeed determined by the chosen gain $K_{\rm x}$. It is then reasonable to assume that the derivative of the estimation for the torque deviation

$$\tilde{\Delta T}_{\rm ij} = \Delta T_{\rm ij} - \hat{\Delta T}_{\rm ij} \tag{45}$$

entering each observer is bounded, so that the following holds

$$|\dot{\tilde{\Delta T}}_{\rm ij}| \leq \dot{\tilde{\Delta T}}_{MAX} \tag{46}$$

Based on this assumption, if the condition (18) is satisfied considering also the effect of the PI adaptation, the system is guaranteed to be stable in spite of the adaptation mechanism.

Assuming the model is correct, the parameters are known and the input signals correspond to the actual ones, the observers converge to the correct estimation, as long as conditions (15) are verified for the models (32) and (43). In order to formalize the convergence properties of the proposed structure, the following reasonable assumptions are made:

(i) All signals entering the observers are bounded, with bounded first derivative;

(ii) The model descriptions adopted are correct, apart from an uncertainty term which represents non captured dynamics and parameter uncertainties. In all cases the uncertainty term is also bounded with bounded first derivative.

Finally, when proving the convergence of the four observers for the longitudinal forces, it is sufficient to consider just one of them, for the generic wheel ij, as the same procedure can be adopted for all the others.

Proposition 1. *Given model* (2) *and estimation law* (16)*,* (19) *applied to the observer defined in* (31)*,* (32)*, a value of the gain* $K_{\rm x}$ *of the S-SOSM input law exists such that the estimation* $\hat{F}_{\rm xw,ij}$ *converges to the real value* $F_{\rm xw,ij}$*, with convergence error depending on the inaccuracy of the estimation* $\hat{\Delta T}_{\rm ij}$ *of the wheel torque deviation.*

Proof. Let us consider the term $\hat{\Delta T}_{\rm ij}$ as an exogenous disturbance with bounded first derivative. This is a reasonable assumption, as it is the output of a PI controller fed by the limited and continuous error $e_{\rm F_x}$ defined in (35). Indeed, the error is limited, since $a_{\rm x}$ is a measurement output and the S-SOSM observers have sufficiently high gains so that the sliding variables $\sigma_{\rm k}$ move towards the origin. Therefore, due to assumption (i) $m\dot{a}_{\rm x}$ is limited, and so is also $\dot{e}_{\rm F_x}$. Let us also assume that the actual dynamics of the wheel are described by model (2), with the dynamic equation of the corresponding observer being (32). Hence, the second derivative of the chosen sliding variable (31) is

$$\begin{aligned}\ddot{\sigma}_{\rm x,ij} &= \ddot{\omega}_{\rm ij} - \ddot{\hat{\omega}}_{\rm ij} \\ &= \frac{1}{J_{\rm w}}(\dot{\tilde{\Delta T}}_{\rm ij} - R_{\rm e}\dot{F}_{\rm xw,ij}) + \frac{R_{\rm e}}{J_{\rm w}}\dot{u}_{\rm x,ij} \\ &= \lambda_{\rm x,ij} + D_{\rm x,ij}\dot{u}_{\rm x,ij}\end{aligned} \tag{47}$$

According to assumption (i) previously made, a bound $\Lambda_{\rm x,ij}$ exists such that $|\lambda_{\rm x,ij}| \leq \Lambda_{\rm x}$ and $D_{\rm x,ij} = D_{\rm x} = \frac{R_{\rm e}}{J_{\rm w}}$. The following inequality can be exploited for the definition of the

bounds for each pair ij:

$$|\lambda_{\mathrm{x,ij}}| \leq \left| \frac{1}{J_{\mathrm{w}}} (\dot{\tilde{\Delta T}}_{\mathrm{ij}} - R_e \dot{F} x w) \right| \leq \frac{1}{J_{\mathrm{w}}} (|\dot{\tilde{\Delta T}}_{\mathrm{MAX}}| + R_e |\dot{F}_{\mathrm{xw_{MAX}}}|) = \Lambda_{\mathrm{x}} \quad (48)$$

Therefore, for a properly chosen gain K_{x}, i.e. a gain choice which enables to generate a SOSM, the convergence is guaranteed $\forall i, j$ ($\dot{\sigma}_{\mathrm{x,ij}} = 0$), leading in finite time (when the system is in sliding condition) to the following estimation

$$\hat{F}_{\mathrm{xw,ij}} = u_{\mathrm{x,ij}} = F_{\mathrm{xw,ij}} + \frac{1}{R_{\mathrm{e}}} \tilde{\Delta T}_{\mathrm{ij}}. \quad (49)$$

□

In order to prove the convergence of the observer for the lateral forces acting on the wheels, it is sufficient to note that the estimation of the F_{xw} forces can be determined from the input of the S-SOSM observers. Then, one has that, as noted in Section III, the following is always bounded

$$\dot{\hat{F}}_{\mathrm{xw_{ij}}} = -K_{\mathrm{x}} sign \left(\sigma_{\mathrm{x_{ij}}} - \frac{\sigma_{\mathrm{x_{ij,MAX}}}}{2} \right) \quad (50)$$

Based on this fact, the following proposition can be formulated.

Proposition 2. *Given model* (3) *and estimation law* (16)*,* (19) *applied to the observer defined by* (42)*,* (43)*, a value of the gain K_y of the S-SOSM input law exists, such that the estimation $\hat{F}_{\mathrm{y,r}}$ converges to the real value $F_{\mathrm{y,r}}$, with convergence error depending on the inaccuracy of the estimation $\hat{\Delta T}_{\mathrm{ij}}$ of the wheel torque deviation plus a component U_{y} which accounts for the unmodelled components of the lateral dynamics.*

Proof. It is here assumed that the real dynamics of the yaw rate are described by (3) plus an additional U_{y} term representing the uncertainties (including parametric ones). Note that here U_{y} is necessary, in contrast with the longitudinal case, since in the latter the uncertainties are already included in the model as ΔT_{ij}, as discussed in Section II. The first equation of (3) then becomes

$$\ddot{\psi} = \frac{1}{J_z} (l_{\mathrm{f}} F_{\mathrm{yb,f}} - l_{\mathrm{r}} F_{\mathrm{yb,r}} + \frac{1}{2} b_{\mathrm{f}} \Delta F_{\mathrm{xb,f}} + \frac{1}{2} b_{\mathrm{r}} \Delta F_{\mathrm{xb,r}}) + U_{\mathrm{y}} \quad (51)$$

Since the observer used is the one described in (43), the second derivative of the chosen sliding variable (42) is

$$\begin{aligned} \ddot{\sigma}_{\mathrm{y}} &= \ddot{r} - \ddot{\hat{r}} \\ &= \frac{1}{J_z} \left[\frac{b_{\mathrm{f}}}{2} (\Delta \dot{F}_{\mathrm{xb,f}} - \Delta \dot{\hat{F}}_{\mathrm{xb,f}}) + \frac{b_{\mathrm{r}}}{2} (\Delta \dot{F}_{\mathrm{xb,r}} - \Delta \dot{\hat{F}}_{\mathrm{xb,r}}) \right] + \\ &\quad - \frac{(l_{\mathrm{f}} + l_{\mathrm{r}})}{J_z} \dot{F}_{\mathrm{y,r}} + \dot{U}_{\mathrm{y}} + \frac{(l_{\mathrm{f}} + l_{\mathrm{r}})}{J_z} \dot{u}_{\mathrm{y}} \\ &= \lambda_{\mathrm{y}} + D_{\mathrm{y}} \dot{u}_{\mathrm{y}} \end{aligned} \quad (52)$$

where $r = \dot{\psi}$. Similarly to the longitudinal case, thanks to assumption (i), one can say that a bound Λ_{y} exists such that $|\lambda_{\mathrm{y}}| \leq \Lambda_{\mathrm{y}}$, while $D_{\mathrm{y}} = \frac{(l_{\mathrm{f}} + l_{\mathrm{r}})}{J_z}$. Therefore, assuming a sufficiently high K_{y} is selected, the convergence is guaranteed. The following inequalities are then defined for the bounds:

$$\begin{aligned} |\lambda_{\mathrm{y}}| &= \frac{1}{2J_z} \left| b_{\mathrm{f}} (\Delta \dot{F}_{\mathrm{xb,f}} - \Delta \dot{\hat{F}}_{\mathrm{xb,f}}) + b_{\mathrm{r}} (\Delta \dot{F}_{\mathrm{xb,r}} - \Delta \dot{\hat{F}}_{\mathrm{xb,r}}) \right| \\ &\quad - \frac{l_f + l_r}{J_z} \dot{F}_{\mathrm{y,r}} + \dot{U}_{\mathrm{y}} \\ &\leq 2 \frac{b_{\mathrm{f}} + b_{\mathrm{r}}}{J_z} (K_x + |\dot{F}_{\mathrm{x,r_{MAX}}}|) + \frac{l_f + l_r}{J_z} |\dot{F}_{\mathrm{y,r_{MAX}}}| + \\ &\quad + |\dot{U}_{\mathrm{y_{MAX}}}| = \Lambda_{\mathrm{y}} \end{aligned} \quad (53)$$

This leads in finite time to the following value for the estimation

$$u_{\mathrm{y}} = \hat{F}_{\mathrm{yb,r}} = F_{\mathrm{yb,r}} + \xi \quad (54)$$

where

$$\xi = - \frac{1}{2R_{\mathrm{e}}(l_{\mathrm{f}} + l_{\mathrm{r}})} \left[b_{\mathrm{f}} (\tilde{\Delta T}_{\mathrm{x,fl}} - \tilde{\Delta T}_{\mathrm{x,fr}}) + \right. \\ \left. - b_{\mathrm{r}} (\tilde{\Delta T}_{\mathrm{x,rr}} - \tilde{\Delta T}_{\mathrm{x,rl}}) \right] - \frac{J_z}{l_{\mathrm{f}} + l_{\mathrm{r}}} U_{\mathrm{y}} \quad (55)$$

□

In order not to overcomplicate the notation, in (55) the effect of the steering angle δ, which numerically, under condition (36), has a much lesser impact compared to the other terms, can be assumed to be included in the uncertainty term U_{y}. The convergence of the front axle force estimation comes as a consequence, based on the second equation in (43).

C. Considerations on the Adaptive S-SOSM Observer

Besides the guaranteed stability and convergence properties, which were illustrated in the previous subsection, the convenience of inserting the adaptive loop in the double observer structure lies in the intrinsic property of disturbance rejection, which characterizes all SM controllers. As a matter of fact, the introduction of the additional adaptive feedback loop does not constitute an issue with respect to both stability and convergence time.

To better illustrate the latter fact, in Fig. 5 the dependence of the upper bound for the convergence time $\bar{t}_{\mathrm{r}}$ on the disturbance level is highlighted, based on (25). The values of Λ_{x}, D_{x} adopted are those from Table I, where all the quantities necessary for the determination of the gains K_{x}, K_{y} are estimated based on the experimental data used for the evaluation in Section VII. The first plot in Fig. 5 should be understood as follows: the nominal gain $K_{\mathrm{x,nom}}$ is chosen as the minimum gain K_{x} satisfying (18), based on the nominal estimated bound $\Lambda_{\mathrm{x,nom}}$. Then, one can see how the convergence time increases for values of $|\lambda_{\mathrm{x}}|$ approaching the limit of stability, i.e. $|\lambda_{\mathrm{x}}| \to \Lambda_{\mathrm{x,nom}}$. Since the disturbance introduced by the adaptive mechanism may increase the value of $|\lambda_{\mathrm{x}}|$, one has that the maximum convergence time increases considerably for values of the gain K_{x} right at the limit of stability, but its raise is substantially reduced, even for marginal increases of the gain, e.g. $K_{\mathrm{x}} = 1.5 K_{\mathrm{x,nom}}$. The effect of the disturbance on the convergence time is practically cancelled for values of the gain one order of magnitude higher than $K_{\mathrm{x,nom}}$. This behavior can be explained by the dependency of γ in (25) on the ratio $|\lambda_{\mathrm{x}}| / \Lambda_{\mathrm{x,nom}}$, which was explained in Subection III-B.

Based on this qualitative analysis, then, one can say that in general the introduction of disturbances into the system does

Table I
VEHICLE DATA AND ESTIMATED BOUNDARIES

$R_e[m]$	$J_w[kg \cdot m^2]$	$l_f + l_r[m]$	$J_z[kg \cdot m^2]$	$b_f + b_r[m]$
0.312	1.5	2.62	3300	3.026
$\lvert\dot{F}_{xw_{MAX}}\rvert$	$\lvert\dot{\Delta T}_{MAX}\rvert$	Λ_x	D_x	$\lvert e_{0,x}\rvert_{MAX}$
10^4	3.2478	1500	0.208	70
$\lvert\dot{F}_{y,r_{MAX}}\rvert$	$\lvert\dot{U}_{y_{MAX}}\rvert$	Λ_y	D_y	$\lvert e_{0,y}\rvert_{MAX}$
10^4	3.2478	10	$7.94 \cdot 10^{-4}$	2

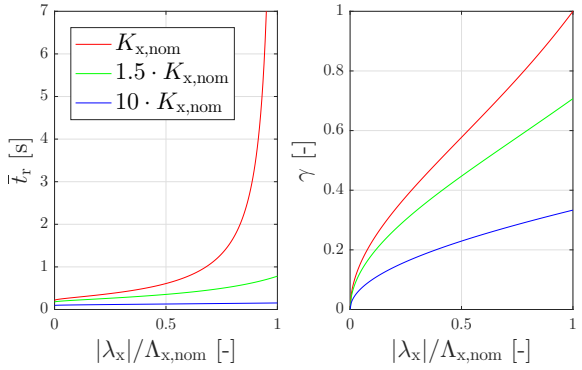

Figure 5. Graphical representation of the convergence time $\bar{t}_r$ (left) and of the quantity γ in (25) (right) depending on the disturbance level expressed as the ratio between $|\lambda_x|$ and its nominal upper bound $\Lambda_{x,nom}$

not lead to an increase in the convergence time. This means that the choice of a value for K_x (and consequently K_y) which is sufficient to dominate the increased disturbance, does not affect significantly the convergence time.

Note that, in the configuration proposed in this paper, a suitably designed EKF is implemented with the purpose of reducing chattering. Therefore, if the noise variance associated with the forces obtained via the SM based virtual sensors (which is dependent on K_x, K_y) is disproportioned compared to that of the measured signals, the covariance matrix R would present a malconditioning problem, possibly resulting in numerical issues during the EKF computation. In practical implementations, thanks to the behavior of $\bar{t}_r$ illustrated above, values for the gains can be chosen so that the malconditioning does not constitute a major problem.

VI. ACCURACY ENHANCEMENT AND LONGITUDINAL FORCES CORRECTION

The S-SOSM observer provides output signals with limited usefulness, due to the possible presence of chattering. Moreover, the most impactful nonlinear phenomena, non captured by the models illustrated in Section II, cause significant deviations in the estimated signals. In this Section the solutions are illustrated, which have been adopted to counter these two problems.

A. EKF Filter

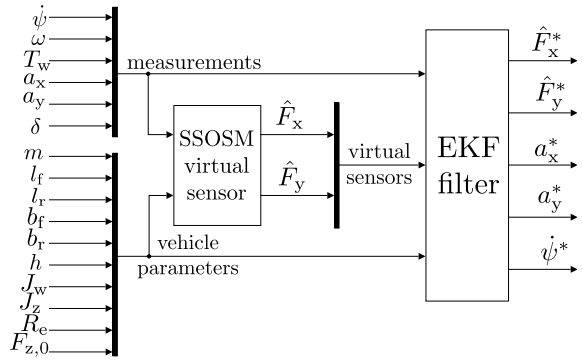

Figure 6. Block diagram of the S-SOSM and EKF structure, in which all signals and vehicle parameters used are highlighted.

When evaluating the signals which are acquired for the forces estimation, one can assume that the measurements of $\dot{\psi}$, a_y, a_x are affected by noise, while driver/vehicle input signals $T_{i,j}$, δ present offset and delays. This fact, in practice, prevents a proper chattering reduction, even in spite of the adoption of the S-SOSM technique with STBA strategy for chattering reduction [30]. A preventive noise cancellation of the measurements would not bring a substantial improvement either: while a pre-filtering of these signals would help smoothing them, it would come at the cost of a substantial phase shift. As a result, the final force estimations would be affected by phase delay and chattering, which is reduced but still not negligible. A second stage of filtering would add further delay, thus making the output signals difficult to use in the target applications.

For all the aforementioned reasons, an EKF is employed, based on the same dynamical representations introduced for the modelling of the longitudinal and lateral vehicle dynamics in Section II. Such device has the goal of smoothing both the estimated forces $F_{xw,ij}$, $F_{yw,ij}$ and the acquired measurement signals $\dot{\psi}$, a_y, a_x. A schematic representation of the S-SOSM/EKF structure is provided in Fig. 6.

Algorithm 1 EKF state estimation

Initialize

$$\hat{\mathbf{x}}(t_0) = E\left[\mathbf{x}(t_0)\right], \quad \hat{\mathbf{P}}(t_0) = Var\left[\mathbf{x}(t_0)\right] \tag{56}$$

Predict-Update

$$\dot{\hat{\mathbf{x}}}(t) = f(\hat{\mathbf{x}}(t), \mathbf{u}(t)) + \mathbf{K}(t)(\mathbf{z}(t) - \mathbf{h}(\hat{\mathbf{x}}(t))) \tag{57}$$

$$\dot{\mathbf{P}}(t) = \mathbf{F}(t)\mathbf{P}(t) + \mathbf{P}(t)\mathbf{F}(t)^T - \mathbf{K}(t)\mathbf{H}(t)\mathbf{P}(t) + \mathbf{Q}(t) \tag{58}$$

$$\mathbf{K}(t) = \mathbf{P}(t)\mathbf{H}(t)^T\mathbf{R}(t)^{-1} \tag{59}$$

$$\mathbf{F}(t) = \frac{\partial \mathbf{f}}{\partial \mathbf{x}}\|_{\hat{\mathbf{x}}(t),u(t)} \tag{60}$$

$$\mathbf{H}(t) = \mathbf{H} = \mathbf{I} \tag{61}$$

The EKF is implemented in the standard form illustrated in Algorithm 1, with the vectors of states $\mathbf{x}$ and inputs $\mathbf{u}$ used in

this representation being defined as:

$$\begin{aligned}\mathbf{x} &= [F_{\mathrm{xw,fl}}, F_{\mathrm{xw,fr}}, F_{\mathrm{xw,rl}}, F_{\mathrm{xw,rr}}, F_{\mathrm{yb,r}}, \dots \\ &\quad a_{\mathrm{x}}, a_y, \omega_{\mathrm{fl}}, \omega_{\mathrm{fr}}, \omega_{rl}, \omega_{\mathrm{rr}}, \dot{\psi}\Big]^{\mathrm{T}} \\ \mathbf{u} &= [T_{\mathrm{fl}}, T_{\mathrm{fr}}, T_{\mathrm{rl}}, T_{\mathrm{rr}}, \delta]^{\mathrm{T}}\end{aligned} \tag{62}$$

Assuming the process and measurement noise $\mathbf{w}$, $\mathbf{v}$ satisfy

$$\mathbf{w} \sim \mathcal{N}(0, \mathbf{Q}), \quad \mathbf{v} \sim \mathcal{N}(0, \mathbf{R}) \tag{63}$$

the following nonlinear continuous state-space description is considered

$$\dot{\mathbf{x}} = \mathbf{f}(\mathbf{x}, \mathbf{u}, \mathbf{w}) \quad \mathbf{y} = h(\mathbf{x}, \mathbf{v}) \tag{64}$$

The nonlinear function $\mathbf{f}(\mathbf{x}, \mathbf{u})$ is the following

$$\mathbf{f}(\mathbf{x}, \mathbf{u}) = [0, 0, 0, 0, 0, 0, 0, f_{x,fl}, f_{x,fr}, f_{x,rl}, f_{x,rr}, f_y] \tag{65}$$

with

$$f_{x,ij} = \frac{1}{J_w}(-R_e F_{xw,ij} + T_{ij}), \tag{66}$$

$$\begin{aligned}f_y &= \tfrac{1}{J_z}(l_f m a_y - (l_f + l_r) F_{yb,r}) + \tfrac{b_f}{2J_z}(\tfrac{F_{xw,fr} - F_{xw,fl}}{\cos(\delta)} + \\ &\quad -2\tan(\delta)\xi_1 \tfrac{a_y}{\xi_2 - a_x}) + \tfrac{b_r}{2J_z}(F_{xw,rr} - F_{xw,rl}).\end{aligned} \tag{67}$$

In order to simplify the notation in (67), ξ_1, ξ_2 have been introduced

$$\xi_1 = \frac{k_f(l_f + l_r)}{b_f(k_f + k_r)} \qquad \xi_2 = \frac{F_{z,f0}}{mh} \tag{68}$$

A lower triangular matrix $\mathbf{F}$ is obtained from the linearization

$$\mathbf{F} = \begin{bmatrix} \mathbf{0}(7,7) & \mathbf{0}(7,5) \\ \mathbf{F}_{5,7} & \mathbf{0}(5,5) \end{bmatrix} \tag{69}$$

with

$$\mathbf{F}_{5,7} = \begin{bmatrix} -\frac{R_e}{J_w} & 0 & 0 & 0 & 0 & 0 & 0 \\ 0 & -\frac{R_e}{J_w} & 0 & 0 & 0 & 0 & 0 \\ 0 & 0 & -\frac{R_e}{J_w} & 0 & 0 & 0 & 0 \\ 0 & 0 & 0 & -\frac{R_e}{J_w} & 0 & 0 & 0 \\ F_{12,1} & F_{12,2} & F_{12,3} & F_{12,4} & F_{12,5} & F_{12,6} & F_{12,7} \end{bmatrix} \tag{70}$$

Elements in the last row of $\mathbf{F}_{5,7}$ are reported in Table II.

Table II
COEFFICIENTS OF THE LINEARIZED MATRIX $\mathbf{F}_{5,7}$

$F_{12,1}$	$F_{12,2}$	$F_{12,3}$	$F_{12,4}$	$F_{12,5}$
$-\frac{b_f}{2J_z\cos(\delta)}$	$\frac{b_f}{2J_z\cos(\delta)}$	$-\frac{b_r}{2J_z}$	$\frac{b_r}{2J_z}$	$-\frac{l_f + l_r}{J_z}$
$F_{12,6}$		$F_{12,7}$		
$-\frac{a_y b_f \xi_1 \tan(\delta)}{J_z(a_x - \xi_2)^2}$		$\frac{l_f m}{J_z} + \frac{(b_f \xi_1 \tan(\delta)}{J_z(a_x - \xi_2)}$		

From a practical point of view, it should be noticed that the standard hypothesis of white gaussian noise are not satisfied for $\mathbf{w}$, $\mathbf{v}$ in (63). For this reason, the tuning of $\mathbf{Q}$ and $\mathbf{R}$, which are effectively the design parameters in the EKF, should be realized with an optimization process. If this approach is followed, given the size of the 2 matrices, in order to reduce the computational burden, the non diagonal elements of $\mathbf{Q}$, $\mathbf{R}$ should be chosen null, i.e.

$$q_{\mathrm{ij}} = r_{\mathrm{ij}} = 0, \quad \forall i \neq j \tag{71}$$

B. Longitudinal Tire-Ground Force Transfer Calculation

The dynamics of a rolling tire have several nonlinearities, resulting from its construction, from the dynamics of rubber or the type of composite materials. For this reason, it is difficult to represent on a real-time basis the full vehicle dynamics. Yet, the adopted simplified model is not well suited to perform accurate state estimation or control. As an example of this fact, values such as the cornering or slip stiffness are usually considered constant for design purposes, while they are time varying parameters which are difficult to estimate in real time.

The resulting longitudinal tire-ground force at the rear wheels is composed by different efforts produced by braking, accelerating or turning. In [19], the concept of "longitudinal tire-ground force transfer" is investigated and defined as the difference between left and right forces, for front or rear axle respectively, i.e.

$$\Delta F_{\mathrm{xw,i}} = F_{\mathrm{xw,il}} - F_{\mathrm{xw,ir}}, \quad i \in \{f, r\} \tag{72}$$

In [20] a modification for the longitudinal tire-ground forces computation is introduced, which yields for each one of the rear wheels

$$F_{\mathrm{xw,rl}} = \xi_{\mathrm{x,rl}} a_{\mathrm{x,rl}} + \xi_{\mathrm{y,rl}} a_{\mathrm{y,rl}} - F_{\mathrm{rr,rl}} - F_{\mathrm{aer,rl}} \tag{73}$$

$$F_{\mathrm{xw,rr}} = \xi_{\mathrm{x,rr}} a_{\mathrm{x,rr}} - \xi_{\mathrm{y,rr}} a_{\mathrm{y,rr}} - F_{\mathrm{rr,rr}} - F_{\mathrm{aer,rr}} \tag{74}$$

with $\xi_{\mathrm{x,rj}}$, $j = l, r$ being a function which depends on the vehicle maneuver (braking or accelerating), the mass and its COG, while $\xi_{\mathrm{y,rj}}$ only depends on vehicle mass and COG position. The variables $a_{\mathrm{x,rj}}$, $a_{\mathrm{y,rj}}$, $j = l, r$, represent the longitudinal and lateral acceleration at the left or right wheel, respectively. $F_{\mathrm{rr,rj}}$ and $F_{\mathrm{aer,rj}}$ represent the rolling resistance and the drag force applied at the specific rear left or right wheel. Thus

$$\begin{aligned}\Delta F_{\mathrm{xw,r}} &= F_{\mathrm{xw,rl}} - F_{\mathrm{xw,rr}} \\ &= \xi_{\mathrm{x,rl}} a_{\mathrm{x,rl}} + \xi_{\mathrm{y,rl}} a_{\mathrm{y,rl}} - F_{\mathrm{rr,rl}} - F_{\mathrm{aer,rl}} \\ &\quad -\xi_{\mathrm{x,rr}} a_{\mathrm{x,rr}} + \xi_{\mathrm{y,rr}} a_{\mathrm{y,rr}} - F_{\mathrm{rr,rr}} - F_{\mathrm{aer,rr}}\end{aligned} \tag{75}$$

The statistical analysis, discussed in [20], puts into evidence ab experimental correlation so that one can claim $\xi_{\mathrm{x,rl}} a_{\mathrm{x,rl}} \approx \xi_{\mathrm{x,rr}} a_{\mathrm{x,rr}}$, $F_{\mathrm{rr,rl}} \approx F_{\mathrm{rr,rr}}$ and $F_{\mathrm{aer,rl}} \approx F_{\mathrm{aer,rr}}$. Then

$$\begin{aligned}\Delta F_{xr} &= \xi_{\mathrm{y,rl}} a_{\mathrm{y,rl}} + \xi_{\mathrm{y,rr}} a_{\mathrm{y,rr}} \\ &= (\xi_{\mathrm{y,rl}} + \xi_{\mathrm{y,rr}})\, a_{\mathrm{y,r}} + (\xi_{\mathrm{y,rl}} - \xi_{\mathrm{y,rr}})\, \dot{\psi}^2 b_{\mathrm{r}}\end{aligned} \tag{76}$$

where b_{r} and $\dot{\psi}$ have already been introduced in Section II. Finally, as variables $\xi_{\mathrm{y,rl}} \approx \xi_{\mathrm{y,rr}}$, the last term in (76) can be neglected, as it does not contribute to explain the longitudinal tire-ground force transfer response. The final expression for (72) is then

$$\Delta F_{\mathrm{xw,r}} = (\xi_{\mathrm{y,rl}} + \xi_{\mathrm{y,rr}}) \cdot a_{\mathrm{y,r}} = \rho_1^{-1} \cdot (F_{\mathrm{y,rl}} + F_{\mathrm{y,rr}}) \tag{77}$$

Table III
CONTROL PARAMETERS

K_{x}	K_{y}	$Q_{F_{\mathrm{x}}}$	$Q_{F_{\mathrm{x}}}$	Q_{ω}	$Q_{\dot{\psi}}$	$Q_{a_{\mathrm{x}}}$
$2 \cdot 10^6$	$2 \cdot 10^3$	26.03	7.68	93.28	77.86	70.35
$Q_{a_{\mathrm{y}}}$	$R_{F_{\mathrm{x}}}$	$R_{F_{\mathrm{y}}}$	$R_{a_{\mathrm{x}}}$	$R_{a_{\mathrm{y}}}$	R_{ω}	$R_{\dot{\psi}}$
8.93	0.25	0.03	0.1	0.05	0.02	2

being ρ_1 a constant parameter greater than the unity, defined as the longitudinal force transfer coefficient, which can be identified from experimental data. Notice that, the assumptions formulated in here are true in the case of regular vehicle designs in which $b_{\mathrm{f}} \approx b_{\mathrm{r}}$.

VII. EXPERIMENTAL ANALYSIS

A. Setup Description

The testbed used to validate in practice the proposals presented here is a 308sw manufactured by Peugeot. This vehicle is instrumented with four wheel force transducers which measure the forces and torques for the x, y and z tire axis. The wheel force transducers also provide, for each wheel ij, the moments M_{z}, M_{x}, M_{y} applied around the three axis, with the latter one corresponding to the applied wheel torque used in the algorithm

$$T_{\mathrm{w,ij}} = M_{\mathrm{y,ij}} \tag{78}$$

The test vehicle is also equipped with an Inertial Measurement Unit (IMU) from which it is possible to obtain the vehicle accelerations (a_x, a_y, a_z) and angular rates ($\dot{\phi}$, $\dot{\theta}$, $\dot{\psi}$). The main sensors and software modules which compose it are shown in Fig. 7.

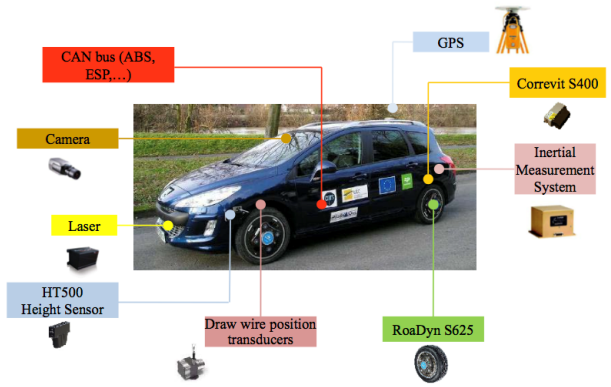

Figure 7. Peugeot 308sw experimental testbed developed at Université de Technologie de Compiègne

B. Results Evaluation

The presented observer is evaluated on a slalom maneuver, which can be divided in three phases: acceleration from standstill (19.5s-27s), cornering (27s-50s) and deceleration to standstill (50s-65s). During the central phase, in which the combined effect of longitudinal and lateral forces is most felt, the vehicle cruise velocity is kept within the $60 - 68$ km/h range. The observer gains K_{X} and K_{y}, as well as the results of the optimization for the values of the diagonal elements of matrices $\mathbf{Q}$ and $\mathbf{R}$, are reported in Table III.

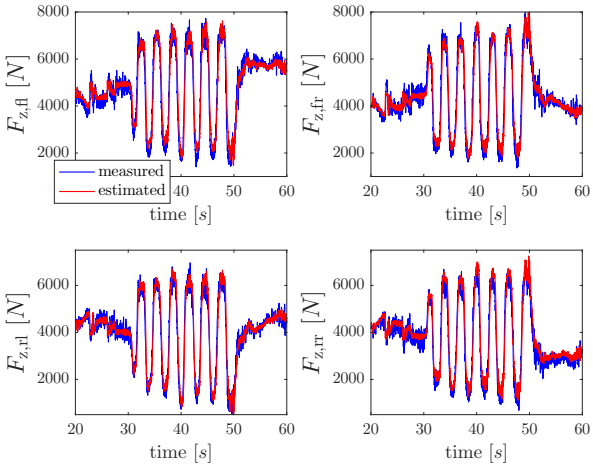

Figure 8. Normal forces estimation

First, the estimation of the normal forces acting on each wheel, based on the static modelling presented in Section II-C, is evaluated. In Fig. 8 it is possible to notice how the normal forces on the wheels $F_{\mathrm{z,ij}}$ are tracked with sufficient accuracy during the entire maneuver. This aspect is important for the subsequent distribution of the lateral forces on the wheels of the same axle.

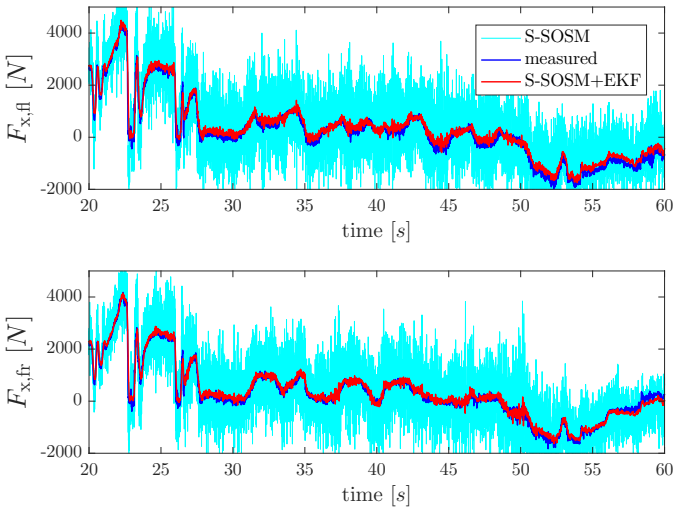

Figure 9. Longitudinal forces estimation: front wheels

The result of longitudinal forces estimation is depicted in Fig. 9 and Fig. 10. In the latter one in particular, which illustrates the forces acting on the rear wheels, one can see how the nonlinear effects compensation, illustrated in Section VI-B, helps identifying with considerable accuracy the rear wheels dynamics. Note that, in the presented results, the "raw" estimation, provided by the S-SOSM observer to the EKF, is also displayed, in order to give a measure of the level of chattering affecting the signals before the filtering.

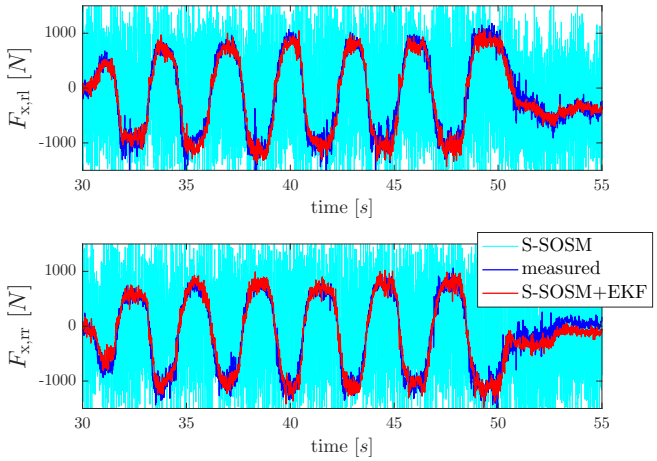

Figure 10. Longitudinal forces estimation: rear wheels

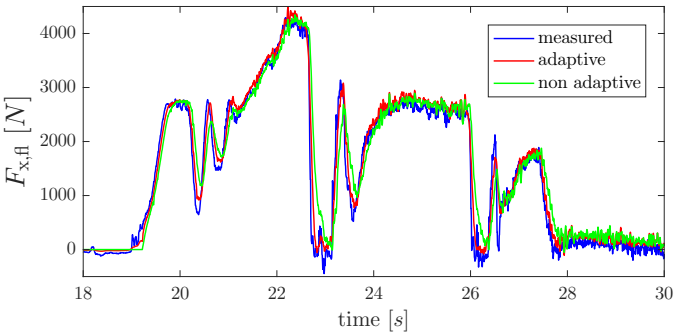

Figure 11. Effect of the adaptive feedback loop with respect to the case in which it is not present

In Fig. 11 a detail of the acceleration phase of the maneuver is depicted, where the effect of the adaptive feedback loop can be appreciated. In the comparison with the S-SOSM observer implemented without adaptation, one can see how, during sharp acceleration phases, the information provided by the accelerometer, more accurate than the one regarding the wheel torque $T_{w,ij}$, helps estimating with more detail the profile of the longitudinal wheel forces.

In Fig. 12 and Fig. 13, the performance of the observer for the lateral forces can be evaluated, for front and rear wheels respectively. The focus in this case is on the central (cornering) phase. One can see, how, despite a small lag introduced by the computations, the tracking is quite accurate, except for deformations in correspondence with the peaks. This minor inaccuracy is due to the force splitting process along the same axle, which in reality is not entirely determined by the distribution of the normal forces, which are in turn estimated correctly, as shown in Fig. 8.

One additional benefit of adopting the EKF structure for the smoothing of the noisy measured signals can be appreciated in Fig. 14, where the acceleration signals, output of the EKF, are compared with the original accelerometer signals. In this case the measurement noise has been cancelled, with almost no introduction of phase delay.

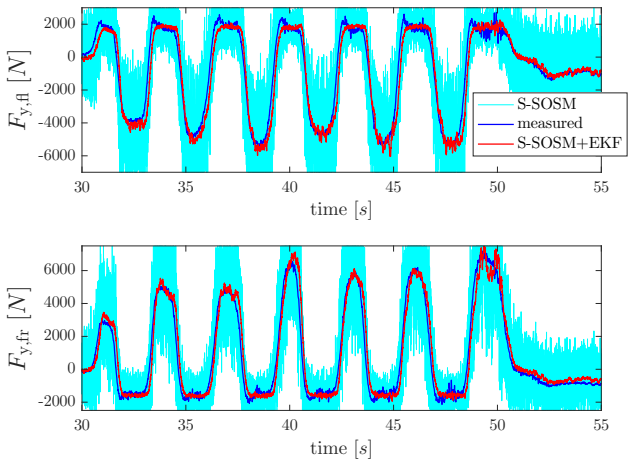

Figure 12. Lateral forces estimation: front wheels

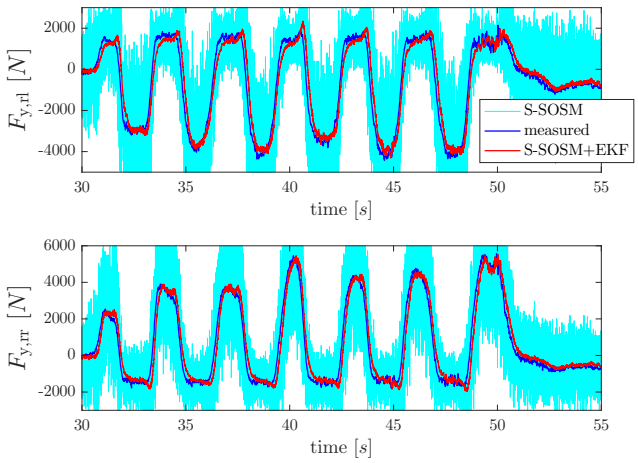

Figure 13. Lateral forces estimation: rear wheels

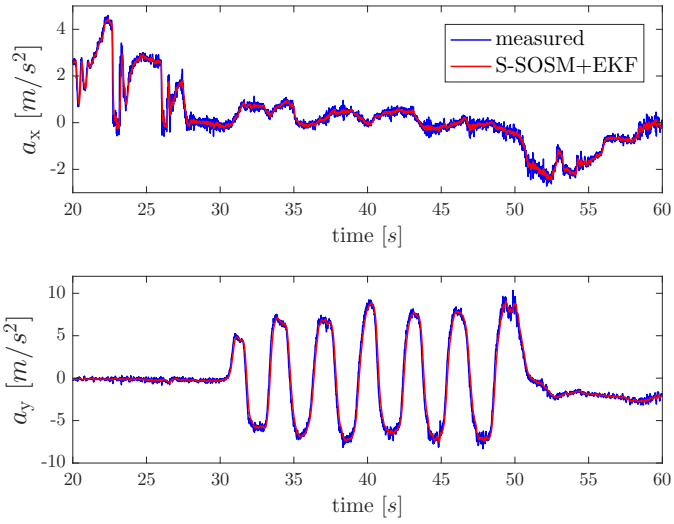

Figure 14. Effect of the proposed S-SOSM+EKF scheme on the accelerometers measurement

VIII. Conclusions

In this article, a tire-ground forces estimation strategy has been proposed, based on Suboptimal Second Order Sliding Mode (S-SOSM) virtual sensors. In the presented implementation, the adoption of the S-SOSM ensures fast convergence and robustness, while an adaptive loop is employed to improve the performance even in the presence of wheel torque measurements which may be inaccurate.

The convergence properties of the structure have also been proven, with qualitative considerations on the effect that the adaptive loop has on the S-SOSM reaching phase. Additionally, an enhanced single track vehicle model allows to allocate the forces on the different wheels, without increasing the complexity of the observer. Finally, the S-SOSM virtual sensor is coupled with an Extended Kalman Filter (EKF), in order to reduce the chattering, while also smoothing the signals obtained from physical sensor measurements.

An experimental validation of the proposed method carried out on a Peugeot 308sw test vehicle at Compiègne, France, has been presented, confirming the validity of the proposal. In the validation phase, an statistical approach is adopted for the inclusion of the main nonlinear phenomena, which are not captured by the enhanced single track model. The results show that the proposed solution can be successfully integrated with the correction based on the statistical approach, thus making this method a valid solution for forces estimation in practical implementations.

Acknowledgement

The project leading to this study has received funding from the European Unions Horizon 2020 research and innovation programme under the Marie Skłodowska-Curie grant agreement No 675999, ITEAM project.

References

[1] J. Pai, "Trends and rollover-reduction effectiveness of static stability factor in passenger vehicles," Mathematical Analysis Division, National Center for Statistics and Analysis, National Highway Traffic Safety Administration, Washington, DC 20509, NHTSA Technical Report: DOT HS 182 444, Report, Jul 2017.

[2] C. Liu and T. J. Ye, "Run-off-road crashes: An on-scene perspective," Mathematical Analysis Division, National Center for Statistics and Analysis, National Highway Traffic Safety Administration 1200 New Jersey Avenue SE., Washington, DC 20590, Report, Jul 2011.

[3] H. K. Fathy, D. Kang, and J. L. Stein, "Online vehicle mass estimation using recursive least squares and supervisory data extraction," in *2008 American Control Conference*, June 2008, pp. 1842–1848.

[4] M. L. McIntyre, T. J. Ghotikar, A. Vahidi, X. Song, and D. M. Dawson, "A two-stage lyapunov-based estimator for estimation of vehicle mass and road grade," *IEEE Transactions on Vehicular Technology*, vol. 58, no. 7, pp. 3177–3185, Sept 2009.

[5] K.-J. Han, I.-K. Kim, and K.-S. H. H Y Jo, "Development and experimental evaluation of an online estimation system for vehicle mass," *Proceedings of the Institution of Mechanical Engineers, Part D: Journal of Automobile Engineering*, vol. 223, no. 2, pp. 167–177, Feb. 2009.

[6] S. Hong, C. Lee, F. Borrelli, and J. K. Hedrick, "A novel approach for vehicle inertial parameter identification using a dual kalman filter," *IEEE Transactions on Intelligent Transportation Systems*, vol. 16, no. 1, pp. 151–161, Feb 2015.

[7] E. Hellström, M. Ivarsson, J. Åslund, and L. Nielsen, "Look-ahead control for heavy trucks to minimize trip time and fuel consumption," *Control Engineering Practice*, vol. 17, no. 2, pp. 245–254, 2009.

[8] B. Ganji, A. Z. Kouzani, and H. Khayyam, "Look-ahead intelligent energy management of a parallel hybrid electric vehicle," in *2011 IEEE International Conference on Fuzzy Systems (FUZZ-IEEE 2011)*, June 2011, pp. 2335–2341.

[9] H. Khayyam, S. Nahavandi, E. Hu, A. Kouzani, A. Chonka, J. Abawajy, V. Marano, and S. Davis, "Intelligent energy management control of vehicle air conditioning via look-ahead system," *Applied thermal engineering*, vol. 31, no. 16, pp. 3147–3160, 2011.

[10] P. Shakouri and A. Ordys, "Nonlinear model predictive control approach in design of adaptive cruise control with automated switching to cruise control," *Control Engineering Practice*, vol. 26, pp. 160–177, 2014.

[11] H. Pacejka and E. Bakker, "The magic formula tyre model," *Vehicle Systems Dynamics*, vol. 21, pp. 1–18, 1993.

[12] H. Dugoff, "Affecting vechicle response to steering and braking control inputs," The University of Michigan, Highway Safety Research Institute, Institute of Science and Technology, Report, May 1969.

[13] L. R. Ray, "Nonlinear state and tire force estimation for advanced vehicle control," *IEEE Transactions on Control Systems Technology*, vol. 3, no. 1, pp. 117–124, 03 1995.

[14] G. Genta, *Motor vehicle dynamics: modeling and simulation*. World Scientific, 1997, vol. 43.

[15] M. Wilkin, W. Manning, D. Crolla, and M. Levesley, "Use of an extended kalman filter as a robust tyre force estimator," *Vehicle System Dynamics*, vol. 44, no. sup1, pp. 50–59, 2006.

[16] G. Baffet, A. Charara, and D. Lechner, "Estimation of vehicle sideslip, tire force and wheel cornering stiffness," *Control Engineering Practice*, vol. 17, no. 11, pp. 1255–1264, 2009.

[17] M. Doumiati, A. Charara, A. Victorino, and D. Lechner, *Vehicle Dynamics Estimation using Kalman Filtering: Experimental Validation*. WILEY, 2012.

[18] A. Rezaeian, R. Zarringhalam, S. Fallah, W. Melek, A. Khajepour, S. K. Chen, N. Moshchuck, and B. Litkouhi, "Novel tire force estimation strategy for real-time implementation on vehicle applications," *IEEE Transactions on Vehicular Technology*, vol. 64, no. 6, pp. 2231–2241, June 2015.

[19] K. Jiang, A. Victorino, and A. Charara, "Robust estimation of vehicle's dynamics states employing a parameter-variable ekf observer," in *2016 IEEE 19th International Conference on Intelligent Transportation Systems (ITSC)*, Nov 2016, pp. 2219–2224.

[20] A. G. Alatorre, A. Victorino, and A. Charara, "Robust multi-model longitudinal tire-force estimation scheme: Experimental data validation," in *2017 IEEE 20th International Conference on Intelligent Transportation Systems (ITSC)*, Nov 2017.

[21] H. Jung and S. B. Choi, "Real-time individual tire force estimation for an all-wheel drive vehicle," *IEEE Transactions on Vehicular Technology*, vol. 67, no. 4, 2018.

[22] A. Ferrara, Ed., *Sliding Mode Control of Vehicle Dynamics*. IET, London, 2017.

[23] A. F. Filippov, *Differential Equations with Discontinuous Right-Hand Sides*, ser. Mathematics and its Applications. Springer Netherlands, 1988, vol. 18.

[24] G. Bartolini, A. Ferrara, and E. Usai, "Chattering avoidance by second-order sliding mode control," *IEEE Transactions on Automatic Control*, vol. 43, no. 2, 02 1998.

[25] E. Regolin, G. P. Incremona, and A. Ferrara, *Sliding mode control of vehicle dynamics*. IET, London, 2017, ch. Longitudinal Vehicle Dynamics Control via Sliding Modes Generation, pp. 33–76.

[26] V. Ricciardi, K. Augsburg, S. Gramstat, V. Schreiber, and V. Ivanov, "Survey on modelling and techniques for friction estimation in automotive brakes," *Applied Sciences*, vol. 7, no. 9, p. 873, 2017.

[27] E. Regolin, D. Savitski, V. Ivanov, K. Augsburg, and A. Ferrara, *Sliding mode control of vehicle dynamics*. IET, London, 2017, ch. Lateral Vehicle Dynamics Control via Sliding Modes Generation, pp. 121–158.

[28] V. Utkin, *Sliding Modes in Control and Optimization*, ser. Communication and control engineering. Springer-Verlag, 1992.

[29] A. Levant, "Sliding order and sliding accuracy in sliding mode control," *International Journal of Control*, vol. 58, no. 6, pp. 1247–1263, Dec. 1993.

[30] E. Regolin, M. Zambelli, and A. Ferrara, "Wheel forces estimation via adaptive sub-optimal second order sliding mode observers," in *2017 XXVI International Conference on Information, Communication and Automation Technologies (ICAT)*. Sarajevo, Bosnia and Herzegovina: IEEE, October. 2017, pp. 1–6.

[31] M. Tanelli, A. Ferrara, and P. Giani, "Combined vehicle velocity and tire-road friction estimation via sliding mode observers," in *Proc. IEEE International Conference on Control Applications*, Oct. 2012, pp. 130–135.

[32] R. Tafner, M. Reichhartinger, and M. Horn, "Estimation of tire parameters via second-order sliding mode observers with unknown inputs," in *13th IEEE Workshop on Variable Structure Systems*, 2014.

[33] A. Pisano, M. Tanelli, and A. Ferrara, "Combined switched/time-based adaptation in second order sliding mode control," *52nd IEEE Conference on Decision and Control*, 2013.

[34] A. Ferrara and G. P. Incremona, "Robust motion control of a robot manipulator via integral suboptimal second order sliding modes," in *Proc. 52th IEEE Conference on Decision and Control*, Dec. 2013, pp. 1107–1112.

[35] R. A. DeCarlo, S. H. Zak, and G. P. Matthews, "Variable structure control of nonlinear multivariable systems: a tutorial," *Proceedings of the IEEE*, vol. 76, no. 3, pp. 212–232, 1988.

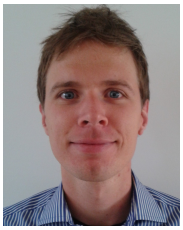

Enrico Regolin received in 2013 the M.Sc. degree in Automation Engineering from the University of Padova. After graduating, he worked for 3 years in AVL as Software Development Engineer in the field of Transmission and Hybrid Powertrains Control. In June 2016 he joined the Identification and Control of Dynamic Systems research laboratory at University of Pavia as doctoral fellow, where his current research interests are sliding mode control and vehicle dynamics control.

Angel Alatorre received in 2014 the M. Sc. degree in automatic control from the center of research and advanced studies from the polytechnic national institute, Mexico City, México. Since 2016, he has been doctoral fellow at the Université de Technologie de Compiègne, France. His current research interests include intelligent vehicles, nonlinear state observers and robust control.

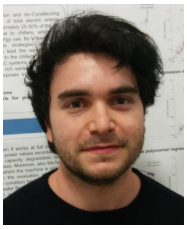

Massimo Zambelli received the B.Sc. degree in Electronics and Computer Engineering and the M.Sc. degree in Computer Engineering from the University of Pavia, Italy, in 2015 and 2017 respectively. He is currently working towards the Ph.D. degree at the University of Pavia. His research interests include automotive control and observers based systems, sliding mode control, and nonlinear robust control.

Alessandro Victorino obtained his M.Sc. degree in mechanical engineering from the State University of Campinas, Brazil, in 1998, and he received his Ph.D. degree from the French National Institute of Automation and Computing Research in Nice, France, in 2002. Since 2006, he has been an Associate Professor in the Computer Science Department, Université de Technologie de Compiègne, France. In 2017 he became a Full Professor in the mechanical engineering department of the Minas Gerais Federal University, in Minas Gerais, Brasil.

Ali Charara received the M.Sc. degree in automatic control from Energie et Traitement de l'information, Institute National Polytechnique de Grenoble, France, in 1988. He obtained his Ph.D. degree in automatic control from the Université de Savoie, at Savoie, France, in 1992. Since 1992, he has been an Assistant Professor in the Department of Information Processing Engineering, Université de Technologie de Compiègne, France. He became a Full Professor in 2003 and he has been the Director of the Heudiasyc Laboratory, Centre National de la Recherche Scientifique during the period 2008-2017.

Antonella Ferrara (S'86-M'88-SM'03) received the M.Sc. degree in electronic engineering and the Ph.D. degree in computer science and electronics from the University of Genoa, Italy, in 1987 and 1992, respectively. Since 2005, she has been Full Professor of automatic control with the University of Pavia, Italy. Her main research interests include sliding mode control applied to automotive systems, process control, and robotics. Dr. Ferrara is a member of the IEEE Technical Committee on Automotive Control and of the IFAC Technical Committee on Transportation Systems.